Bond Graph based control of a three phase inverter with LC filter

Roberto Sanchez[1,3]
Frédéric Colas[2]
Geneviève Dauphin-Tanguy[3]
Xavier Guillaud[1]
(1) L2EP, (3) LAGIS, UMR CNRS 8146, Ecole Centrale de Lille, BP 48, 59651 Villeneuve d'Ascq cedex, France.
(2) ENSAM Lille, Arts et Métiers ParisTech, 8 bd Louis XIV, 59000 Lille cedex, France.
roberto_ts@hotmail.com, frederic.colas@ensam.eu, genevieve.dauphin-tanguy@ec-lille.fr, xavier.guillaud@ec-lille.fr

KEYWORDS

Bond Graph, inverter.

ABSTRACT

In this paper is proposed a model of a three phase electrical inverter with a LC output filter in delta connection used in a renewable energy supply system. The concept of inverse bond graph via bicausality is used for the control law design. The control law is compared in simulation with another traditional one and validated experimentally.

INTRODUCTION

Power systems have been developed over the years to supply a varying demand from centralized generation sources of fossil and nuclear fuels. Nowadays the renewable energy sources start to play an important role in the grid connection, so the renewable sources need to be integrated into the electrical network via electronic power converters.
The electronic power converters are not only used for the connection between a renewable energy source and the network, they are also used in many industrial applications. The multi physics aspect of such systems justifies the bond graph approach.
The bond graph model of a three phase inverter has been addressed in several research papers, as for example for the most recent publications: [Mezghanni et al., 2007; Belhadj, 2006; González-Contreras et al., 2007]. Each presented model has different characteristics and is used for different applications. They have in common that they have been established with an electronic switch (MTF) for modeling the commutation cell of the converter; moreover the different papers used a PWM technique for controlling the commutations in these elements. Here we propose to model the three phase electrical inverter with only two electronic switches [Guillaud & Francois, 2003] and to control it without using PWM method.
For designing the control law, we use the inverse bond graph model using the bicausality concept [Ngwompo et al, 1996]
A specific controller is proposed combining the inverse model and a resonant block.
The outline of this paper follows. In the second section a presentation of the global system is given. In section 3 the bond graph model of a three phase inverter with LC filter is proposed and some causality problems are discussed. A two stage control law for the inverter is given in section 4. Section 5 shows the experimental and simulation results. Finally some conclusions are given.

PRESENTATION OF THE GLOBAL SYSTEM

Figure 1 shows the global scheme of a renewable energy source connected to a load. This structure is the basic one and could be analyzed at different levels of complexity.
The renewable energy source could be a panel of photovoltaic cells, a gas turbine or a wind turbine. It delivers the primary power in the DC bus which will be converted into AC power via the power converter. The introduction of a capacitor on the DC bus is necessary in order to have a decoupling between the harmonics generated by both converters. In this part of the system, it is necessary to make the regulation of voltage (u_s) or current (i_m).

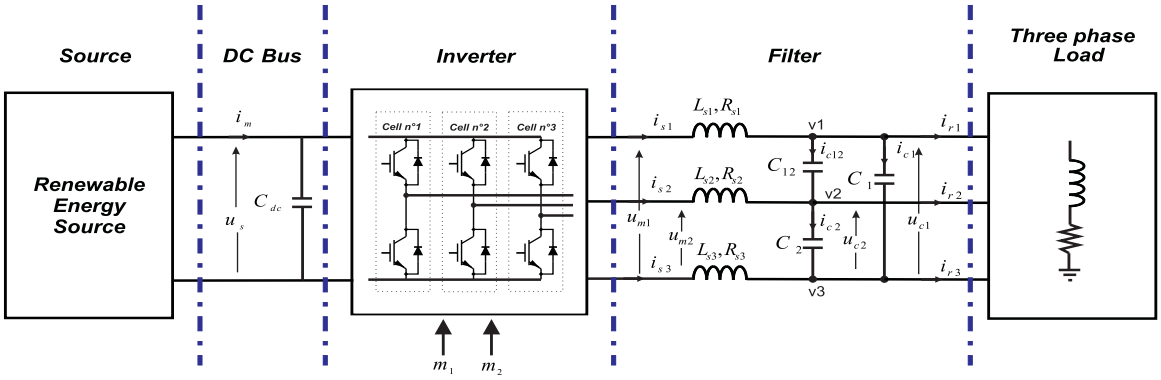

Figure 1 Global electrical system.

Proceedings 23rd European Conference on Modelling and Simulation ©ECMS Javier Otamendi, Andrzej Bargiela, José Luis Montes, Luis Miguel Doncel Pedrera (Editors)
ISBN: 978-0-9553018-8-9 / ISBN: 978-0-9553018-9-6 (CD)

The power electronic converter might be considered as an amplifier. It is composed of three pairs of electronic switches (Mosfet, IGBT, etc.). Each pair of switches is called a commutation cell.
In the filter part, the basic one is known as a LR filter, which consists only in one inductance in series with a resistance; it can be taken as a base for more complex filters, only by adding more components, for example LC one (figure 1) which has one inductance and resistance in series with a capacitor in parallel. Each filter configuration has its own characteristics and is used for specific requirements or analysis from the point of view of stability and harmonics analysis.
In figure 1, the currents in inductances L_{si}, i=1, 2, 3, and the voltages of capacitors C_1, C_2, C_{12} are controlled. Thus, the behavior of this system may be assimilated to a voltage source, contrary to the classical LR filter structure which is assimilated to a current source. The main advantage with such a voltage source is in case of connection to the grid, because it avoids any dependence of the voltage in the C-elements to the voltage grid.
The grid will be chosen here as a passive load (R, L).

MODEL OF THE INVERTER AND THE FILTER

In this paper the model of the inverter shows up explicitly only two of the three commutation cells, the third one fixing the voltage reference. Only 2 phase to phase voltages (u_{m1}, u_{m2}) have to be considered for control [Guillaud & Francois, 2003]. The current i_{s3} is linearly dependent of the two others (i_{s1} and i_{s2}).
We are focusing on the average behavior of the converter. Furthermore, we are not interested in the switches themselves, but on the impact of the converter on the LC filter.
Thus, we define 2 control signals (m_1, m_2) which are defined as:

$$m_1 = \frac{u_{m1}}{u_s} \quad \text{and} \quad m_2 = \frac{u_{m2}}{u_s} \qquad (1)$$

The primary source of the converter in the DC bus is represented as a constant voltage source (u_s) by assuming that it has no variation or fluctuation.
The three phase LC filter is composed of three inductances with their associated resistance and three Delta connected capacitors.
The model is made in two stages. Firstly, the three inductances and their associated resistances are taken into consideration; secondly the three capacitors are added.
The three phase inverter model with the LR filter is shown figure 2. The element I: L_{s3} has a derivative causality because of the 0-junction placed between the bonds 21, 22 and 23, which represents the Kirchhoff law (sum of the currents equal to zero).

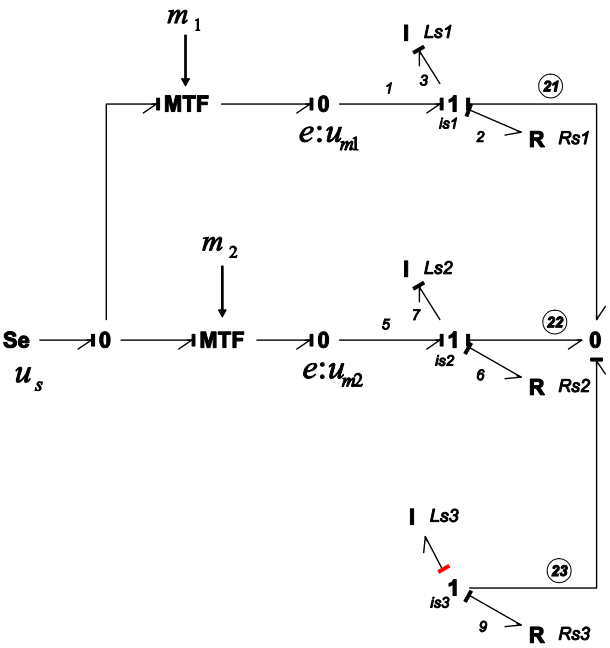

Figure 2 Bond Graph model of the three phase inverter with a LR filter.

Taking the bond graph of figure 2 as base, the three C-elements are added (figure 3).

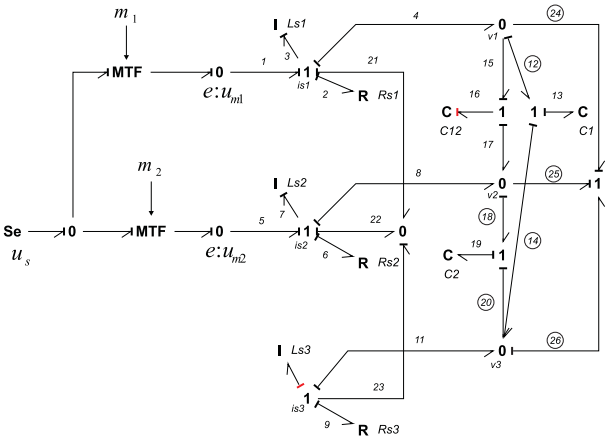

Figure 3 Bond Graph model of the three phase inverter with a LC filter.

In figure 3 the element C: C_{12} has a derivative causality because of the 1- junction linking bonds 24, 25 and 26, which represents the Kirchhoff law (sum of the voltages equal to zero).
The bond graph model shows up two causality loops (following effort and following flow) in bonds 24, 26, 14, 12, and two others in bonds 25, 26, 20, 18 [Van Dijk & Breedveld, 1991], each of them with a gain equal to minus one. Thus, the model can be simulated. These causality loops are introduced because of the configuration in Delta connection of the capacitors. In a star connection they would not exist.
The bond graph model explicitly points, out the physical insight of the system with the two elements in derivative causality (L_{s3} and C_{12}).

Finally, figure 4 shows the connection of L-R elements (load) for each branch.

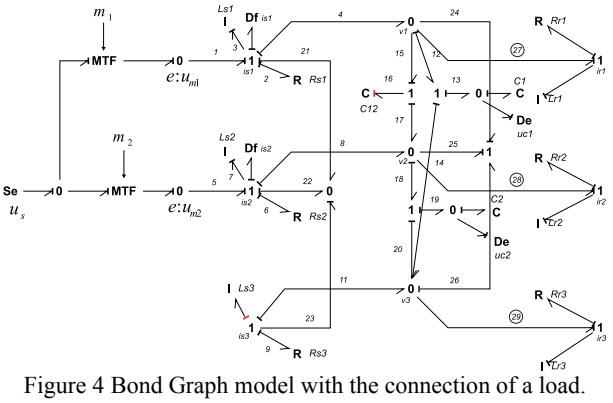

Figure 4 Bond Graph model with the connection of a load.

Elements L and R in bonds 24, 25 and 26 are assigned with integral causality.
The four detectors (Df: i_{s1}, Df: i_{s2}, De: u_{c1}, De: u_{c2},) shown in figure 4 are associated with the sensors.

CONTROL OF THE INVERTER AND THE FILTER

In this section we propose a new control structure for the three phase converter, and we recall a classical one which will be used for comparison purpose.

Control via inverse model and bi-causality bond graph

The control law applied to the model is based on the bi-causality bond graph, and is designed from the inverse bond graph.
The notion of bicausality was introduced by Gawthrop [Gawthrop, 1995], and can be used to point out properties about inverse dynamics [Ngwompo et al, 1996] and parameter estimation [Ngwompo & Scavarda, 1999].
For the formulation of the inverse bond graph, it is necessary to change the flow detectors Df (supposed ideal) of the original bond graph for sources (named Se_0Sf, because they impose to the inverse model zero effort-non null flow), then propagate the bicausality (in only one line of power transfer) from this source (SS) to the input source of the original bond graph which becomes a detector in the inverse bond graph [Ngwompo et al, 1996].
With the inverse bond graph we design the structure of the control in open loop, which is then extended to a closed loop control by fixing the dynamics of the errors.
The three phase voltages have to be controlled. However, there are two different ways to proceed:
- The first way assumes that the dynamics in the I: L_{si} elements are faster, compared with the dynamics in the C-elements. Thus only the voltages in C_1 and C_2 are controlled in closed loop; the voltage in the dependent C_{12} element is directly related to the two others.
- The other way considers the two loops in cascade, one for the current in the L_{si} and another one for the voltage in C_i-elements. In this paper, we choose to make the control law via the two closed loops, for performance purpose.

The calculation of the control laws in the model is made in two steps, the first one for the currents and the next one for the voltages.
The figure 5 shows up the inverse bond graph, which allows deducing the open loop current control law. The two current sensors are inverted simultaneously via bi-causal bonds and two disjoint bicausal paths are drawn to the two desired inverse model outputs corresponding to the two control signals (m_1, m_2), which proves that the model is invertible [Ngwompo et al, 1996].

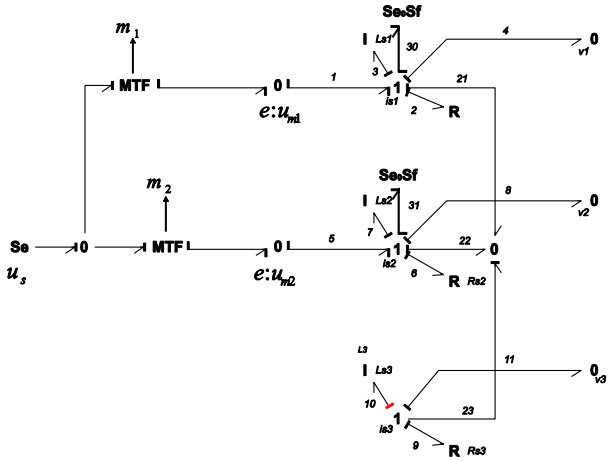

Figure 5 Inverse bond graph for the calculation of the current control law.

The I-elements are in derivative causality. Equation (2) is derived from the inverse bicausal bond graph of figure 5, by setting that the numerical values of R_{si} and L_{si} are the same for the 3 phases. It gives:

$$\begin{pmatrix} m_1 \\ m_2 \end{pmatrix} = \left(\frac{1}{u_s}\right)\left(\left(R_s + L_s\frac{d}{dt}\right)\begin{pmatrix} 2 & 1 \\ 1 & 2 \end{pmatrix}\begin{pmatrix} i_{s1} \\ i_{s2} \end{pmatrix} + \begin{pmatrix} u_{c1} \\ u_{c2} \end{pmatrix}\right) \quad (2)$$

For establishing the closed loop control law, we set up the dynamics of the error ($\varepsilon_i = i_{sref_i} - i_{s_i}$) in both expressions, as $\dot{\varepsilon}_i + k_{p1}\varepsilon_i = 0$, where k_{p1} is a constant gain to be fixed. The expression (2) becomes (3) as

$$\begin{pmatrix} m_1 \\ m_2 \end{pmatrix} = \left(\frac{1}{u_s}\right)\left(\left(R_s + L_s\frac{d}{dt}\right)\begin{pmatrix} 2 & 1 \\ 1 & 2 \end{pmatrix}\begin{pmatrix} i_{s1ref} - \varepsilon_1 \\ i_{s2ref} - \varepsilon_2 \end{pmatrix} + \begin{pmatrix} u_{c1} \\ u_{c2} \end{pmatrix}\right) \quad (3)$$

Finally,

$$\begin{pmatrix} m_1 \\ m_2 \end{pmatrix} = \left(\frac{1}{u_s}\right)\left(\begin{pmatrix} 2 & 1 \\ 1 & 2 \end{pmatrix}\left(R_s\begin{pmatrix} i_{s1} \\ i_{s2} \end{pmatrix} + L_s\frac{d}{dt}\begin{pmatrix} i_{s1ref} \\ i_{s2ref} \end{pmatrix} + k_{p1}\begin{pmatrix} i_{s1ref} - i_{s1} \\ i_{s2ref} - i_{s2} \end{pmatrix}\right) + \begin{pmatrix} u_{c1} \\ u_{c2} \end{pmatrix}\right) \quad (4)$$

As for the determination of the current control, the voltage control law is calculated; it provides the current reference for equation (4). Figure 6 shows the inverse

bond graph used for the determination of the current reference.

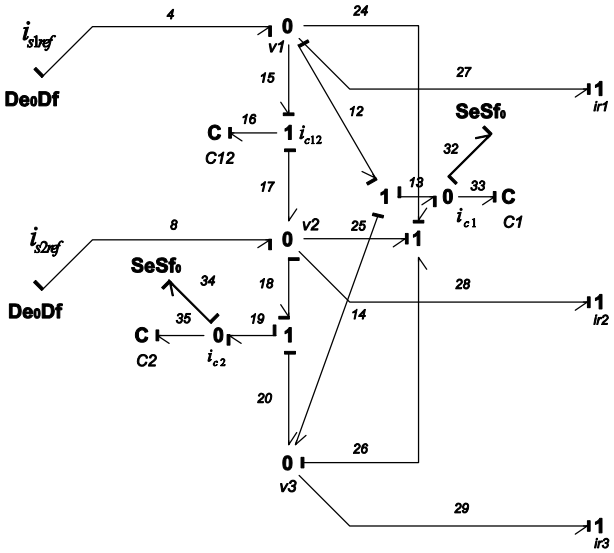

Figure 6 Inverse Bond Graph for the voltage control law.

For deriving equation (5) from figure 6, we follow the same procedure as previously. Two bicausal disjoint paths exist from one $SeSf_0$ to one De_0Df. The model is thus invertible. It leads to

$$\begin{aligned} i_{s1ref} &= C\frac{d}{dt}\left(2u_{c1}-u_{c2}\right)+i_{r1} \\ i_{s2ref} &= C\frac{d}{dt}\left(2u_{c2}-u_{c1}\right)+i_{r2} \end{aligned} \tag{5}$$

According to the fact that the 3 capacitors are supposed with the same values capacitances, thus equations (6) show up the voltage control law for the converter.

$$\begin{pmatrix} i_{s1ref} \\ i_{s2ref} \end{pmatrix} = \begin{pmatrix} 2 & -1 \\ -1 & 2 \end{pmatrix} \left(C\frac{d}{dt}\begin{pmatrix} u_{c1ref} \\ u_{c2ref} \end{pmatrix} + Ck_{p2}\begin{pmatrix} u_{c1ref}-u_{c1} \\ u_{c2ref}-u_{c2} \end{pmatrix} \right) + \begin{pmatrix} i_{r1} \\ i_{r2} \end{pmatrix} \tag{6}$$

In equations (4) and (6), k_{p1} and k_{p2} are constant gains to be fixed. We choose to change k_{p2} for a resonant controller given equation (7) [Sato et al., 1998; Guillaud et al., 1999]:

$$\left(\frac{n_2 s^2 + n_1 s + n_0}{s^2 + \omega_n^{\,2}} \right) \tag{7}$$

In (7), the natural frequency (ω_n) is adjusted to the input signal frequency in order to obtain an infinite open loop gain at this frequency [Lopez de Heredia et al., 2006].
The calculation of the parameters in the resonant controller is made using the pole placement approach [Leclercq, 2004].
On the other hand, the gain k_{p1} is calculated for each phase by placing the pole of the polynomial denominator of the transfer function in closed loop derived from Figure 7. The desired performances for the closed loop model are given hereafter.

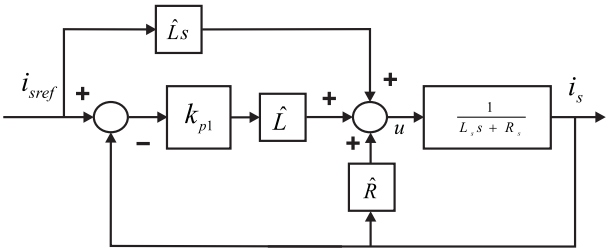

Figure 7 Block diagram for the current loop.

In figure 7, elements $\hat{L}$ and $\hat{R}$ are estimated values of the actual system parameters.
The controller block diagram of the complete model is shown in figure 8. It is important to notice that the structure of the control law contains a feed-forward with a derivative action on the references. The reference signals are sinusoidal and they can be derived analytically without any problem. The proposed control law is compared by simulation with a classical one described hereafter.

Control via Park transformation

A classical control approach consists in transforming the sinusoidal reference into a continuous reference by applying a framework change using the Park transformation. By this way, a classical proportional integral controller can be used without any problem, the resonant controller having no meaning here because of the constant value of the reference signals. As for the control previously presented, the control via Park transformation uses the two loop cascade control structure. Figure 9 shows the structure of the controllers.

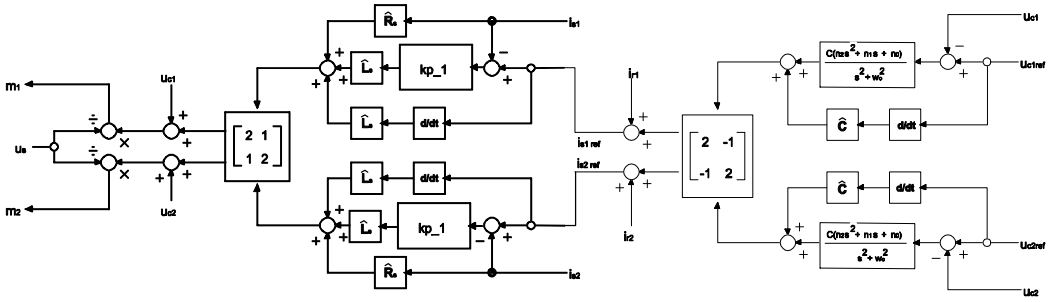

Figure 8 Inverse model Controller block diagram in sinusoidal reference.

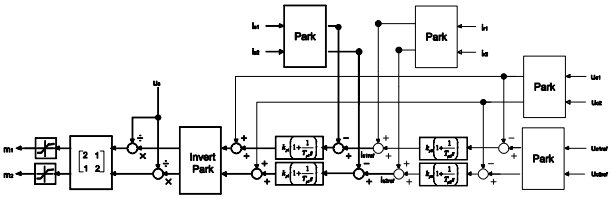

Figure 9 PI Controller block diagram in Park reference.

Simulation and experimental results of the two systems are shown in next section.

EXPERIMENTAL AND SIMULATION RESULTS

a) Simulation

The simulation results are obtained with the software 20Sim®.
The table 1 shows the numerical values used in the model.

Table 1 Numerical parameters for the system and control.

System
$L_s = 0.55mH \;\; R_s = 0.22\Omega \;\; C = 22\mu F \;\; R_r = 645\Omega$
Values for inverse control law
$\hat{L}_s = 0.5mH \;\; \hat{R}_s = 0.2\Omega \;\; \hat{C} = 20\mu F$
$n_2 = 0.072 \;\; n_1 = 43.2 \;\; n_0 = 11009 \quad k_{p1} = 2000$
Values for Park control law
$k_{p1} = 2.425 \;\; T_{p1} = 2.46e-4 \;\; k_{p2} = 0.0336 \;\; T_{p2} = 1.2e-3$

For the two models the references are two sinusoidal signals with 340 volts amplitude and 50Hz frequency, diphased of 120°.
The numerical values of table 1 have been calculated taking a time response of 10 ms in the voltage loops and 1 ms in the current ones.
Figures 10 and 11 show the simulation responses in one phase for the two closed loop models, when one step load change is made at time = 0.544 s. The load is balanced (same L and R parameter values in the three phases).

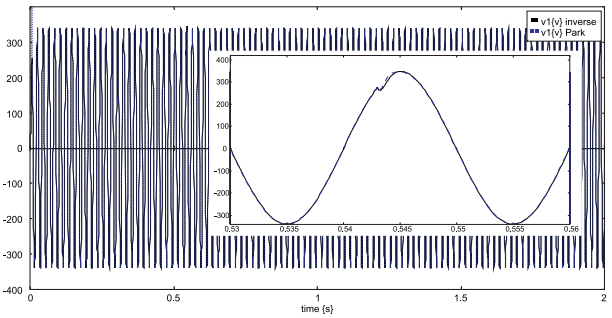

Figure 10 Simulation: voltage in one C-element – balanced load

In figure 10, no change appears in the voltages. In the opposite, the figure 11 shows the change in the filter current responses.

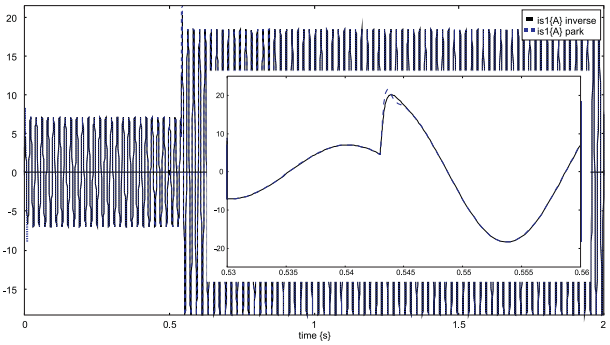

Figure 11 Simulation filter current results.

Finally, in figure 12 is presented the load current.

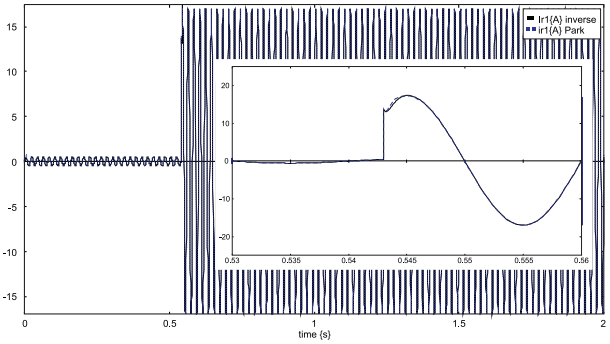

Figure 12 Simulation: current in the load – balanced load

We obtain the same responses in both control structures because the same time response has been considered.
Consider now the case of an unbalanced load (third phase L and R parameter values different from the two others). Figure 13 shows the responses obtained for the control law with PI controllers in Park reference, and figure 14 for the responses from the proposed inverse model controller.

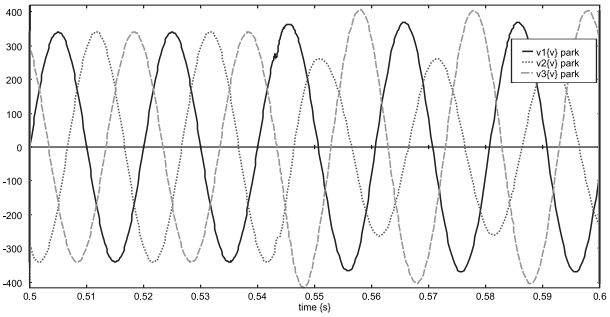

Figure 13 Simulation: voltages in C-elements for an unbalanced load - PI controllers in Park model.

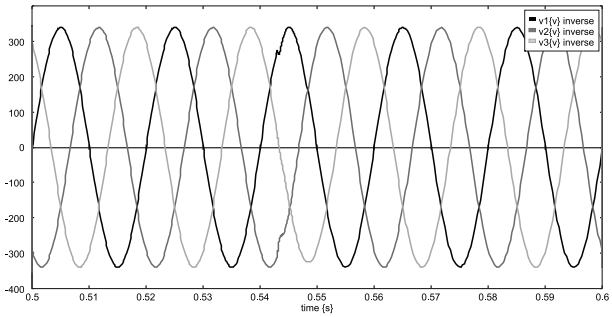

Figure 14 Simulation voltage results for an unbalanced load - inverse model controller - sinusoidal reference.

It is shown that the inverse model control has a better behavior compared to the PI one in the Park reference. Experimental implementation (as shown hereafter) confirms the robustness of the proposed new control law versus parameter uncertainties.

b) Experimentation

For the experimental implementation, we used a real time simulator as shown figure 15.

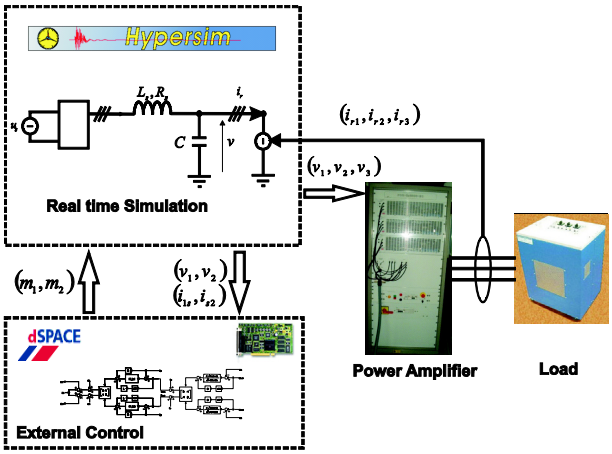

Figure 15 Scheme of the experimental set up.

The capacitor voltages (v_1, v_2, v_3) are transmitted to the high bandwidth power amplifier which applies the voltages to the load.

The currents flowing into the load are measured and introduced in the real time simulation model via an ADC (analogical to digital converter). The effect of the load is introduced in the real time simulator as a three phased current source.

For the experimental results, we considered the same numerical values as for the simulation (table 1).

We show up the responses for the voltage and currents for a LR series load. The reference voltage is 240 volts RMS and a three phase resistive load of 645 Ω with unbalanced inductances (0.1H, 0.107H and 0.08H). We applied one step change in the 3 R values (120 Ω) at 0.054 seconds. The three phase voltages are shown in figure 16.

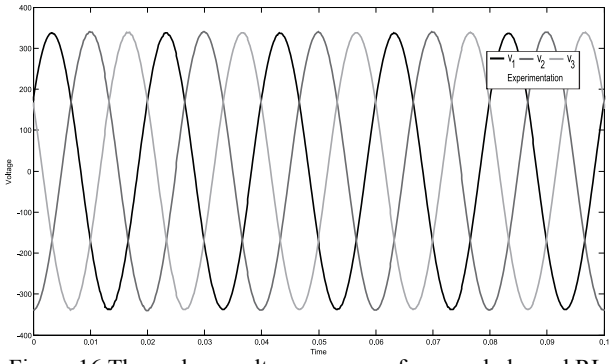

Figure 16 Three phase voltage response for an unbalanced RL load.

As expected, we can notice in the figure 16 that the change in the load has no impact on the voltages. In the opposite, the actual change can be seen in the three load currents (figure 17).

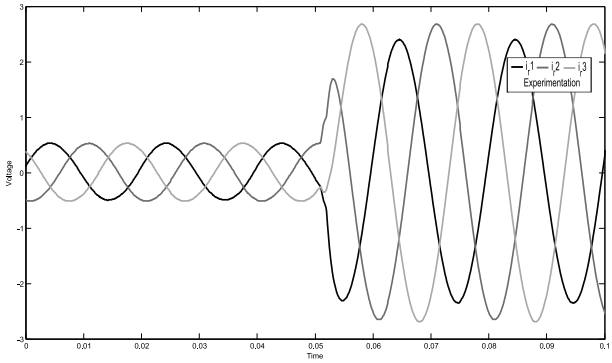

Figure 17 Responses of the currents for an unbalanced RL load – step change in load R values at 0.054s

The unbalancing of the load due to a different value of the inductance in the phase 1 appears explicitly. In addition, for the filter currents (figure 18) we can notice a little change in the magnitude at time 0.054s. The perturbations in the signals are due to measurement noises.

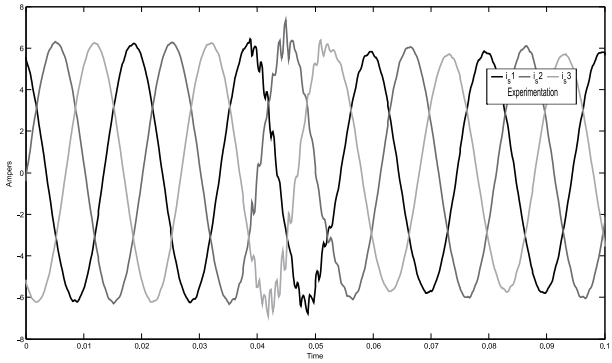

Figure 18 Responses of the currents in the filter, for an unbalanced RL load.

The experimental results have been compared with the simulation results and we found that they are very similar.

CONCLUSIONS

A new bond graph model of a three phase inverter coupled with a LRC filter has been proposed. This model keeps the three branches of the AC current side and uses only two elements for the commutation of the inverter. Moreover, we proposed a new structure for the control law derived from the inverse bond graph using the concept of bicausal bond graphs. It has been shown through simulation and experimentation that the proposed control structure is robust versus parameter deviations.

The future developments will consist in connecting active loads to the system, such as an asynchronous machine.

ACKNOWLEDGEMENT

The authors would like to thank the support given by the Conacyt, Mexico.

REFERENCES

Belhadj J. 2006. *Modeling, Control and Analysis of Multi-Machine Drive Systems using Bond Graph Technique*. Journal of Electrical Systems 2-1, pp 29-51.

Gawthrop P. 1995. *Physical Model-based Control: A Bond Graph Approach*. Journal of the Franklin Institute, volume 332B, No. 3, pp. 285-305.

Gawthrop P. 1995. *Bicausal Bond Graph*, (1995) In Proceeding of the International Conference on Bond Graph Modeling and Simulation ICBGM'95, vol. 27, pp. 83-88.

González-Contreras B.M., Rullán-Lara J.L., Vela-Valdés L.G., Claudio S.A. 2007. *Modelling, Simulation and Fault Diagnosis of the Three-Phase Inverter Using Bond Graph*. IEEE International Symposium on Industrial Electronics.

Guillaud X., Vandecasteele F., Wulverick M., Hautier J.P. 1999. *New concept of corrector for the control of alternatives quantities*. Proc. 8th European Conference on Power Electronics, EPE Lausanne.

Guillaud X., Francois B. 2003. *A causal method for the modeling of static converter and the control design. Application to a Voltage Source Converter*. 10th European Conference on Power Electronics and Applications, EPE 2003, 2-4.

Leclercq L. 2004. *Apport du stockage inertiel associé à des éoliennes dans un réseau électrique en vue d'assurer les services systèmes*. These USTL Lille.

Lopez de Heredia A., Gaztañaga H., Etxeberria-Otadui I., Bacha S., Guillaud X. 2006. *Analysis of Multi-Resonant Current Control Structure and Tuning Methods*. IEEE Industrial Electronics, IECOM 2006, pp. 2156-2161.

Mezghanni D., Andoulsi R., Mami A. and Dauphin-Tanguy G. 2007. Bond *graph modeling of a photovoltaic system feeding an induction motor-pump*. Simulation Modelling Practice and Theory, pp 1224-1238.

Ngwompo R.F., Scavarda S., and Thomasset D. 1996. *Inversion of Linear Time-invariant SISO Systems Modelled by Bond Graph*. Journal of the Franklin Institute, Vol. 333(B), No. 2, pp. 157-174.

Ngwompo R.F., Scarvarda S. 1999. *Dimensioning problems in system design using bicausal bond graph*. Simulation Practice and Theory, pp 577-587.

Sato Y., Ishizuka T., Nezu K., Kataoka T. 1998. *A new control strategy for voltage-type PWM rectifiers to realize zero steady-state control error in input current*. IEEE Transaction on Industry Applications, vol. 32, issue 3, pp 480-486.

Van Dijk J. and Breedveld P. 1991. *Simulation of system models containing zero-order causal paths I. Classification of zero-order causal paths*. Journal of the Franklin Institute, 328 (5/6), pp. 959-979.